3D Particle Position Measurement via the Defocusing Concept

Xiaoli Bao, Muguo Li
State Key Laboratory of Coastal and Offshore Engineering, Dalian University of Technology, Dalian 116024, China
E-mail: echo_allen@hotmail.com

Abstract

This paper presents a 3D particle position measurement method based on the defocusing concept introduced by A.Pentland with a single camera. Different from the existing approaches, the blur circle is used to identify the blur extent for various defocused particles, and the depth-blur relation is formulated by the modified A.Pentland mathematical formula. And, an eight-step algorithm based on Circular Hough Transform and Quadrant Radius Histogram was given to calculate the 3D particle position. Experiments on real defocused particle images have demonstrated the feasibility of the proposed method for 3D particle position recovery, and the minimum Mean Absolute Error of depth is about 0.18 mm.

Keywords: *particle position measurement; Circular Hough Transform; Quadrant Radius Histogram.*

1. Introduction

Particle Image Velocimetry (PIV) has developed to the stage of measurement of 3D velocity components in 3D flow fields. As a result, lots of 3D PIV techniques have been investigated. Many of them are base on seeding particles, which visualize the flow and can be recorded by an imaging system. 3D particle position measurement of tracer particle becomes one of the essential problems in 3D PIV research. Although, various approaches are proposed for determining particle 2D position in object plane, particle depth measurement is not well established yet.

The stereoscopic 3D particle position measurement approach requires at least two, but rather three or four synchronized cameras [1][2]. The configuration of a multi-camera system may pose financial and technical challenges. Holographic approach has received much attention [3][4], praised for their high potential but reluctantly implemented due to their delicate optical set-up and sensitivity to environment perturbations. The defocusing approach, unlike stereoscopic approaches, has one unique optical axis and is based on pattern matching rather than on stereoscopic matching of particle images [4]. Originally, a single camera with a modified three-hole aperture was used [5]. Due to the pinhole mask, there exists the problem of a significant lack of illumination in a conventional lighting setup. Lately, three individual cameras are used instead of pinhole mask [6]. Some simulations using synthetic images show that particle density should be lower than 0.01 particles per pixel. Particle image shape is used by Hain and Kähler [7]. Anastigmatic imaging lens produces ellipsoidal particle images whose elongation and orientation depend on the separation of the particle from the plane of best focus. The implementation of these two techniques was discussed in μ PIV [8].

It is well known that defocus blur of a point object depends on aperture size if the focal length and depth are fixed [9]. When the lens aperture was set at f /4, one experimental defocused particle image in the illuminated volume (about 3 cm thick) was acquired and shown in Fig. 1.

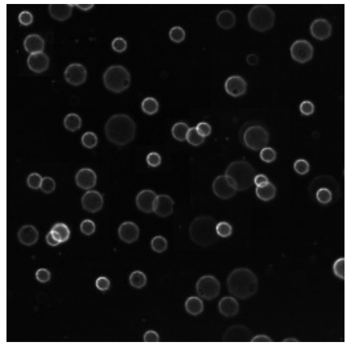

Figure 1 Experimental defocused particle image

One interesting discernible point which can be noticed in Fig. 1 is that the defocused particles are hollow blur circles and have sharp edges. So, 2D Gaussian function is not a good model of point-spread function for defocusing [10][11]. It is possible to use a blur circle, instead of using a 2D Gaussian function, to describe the defocused particle.

In this paper, we present a 3D particle position measurement method based on depth from particle defocus [12]. 3D particle position can be calculated directly using the mathematical formula without correspondence problem and expensive calculation.

The remainder of the paper comprises four sections. Section 2 reviews the measurement principles based on particle defocus. Section 3 represents the basic theories used in this study. Section 4 explains the procedure for calculating the 3D particle position. Section 5 presents the experimental results. Section 6 concludes the paper.

2. Measurement principles

A typical imaging system is represented in Fig. 2. In Fig. 2, v_0 is the distance between the image plane and the lens, u_0 is the distance between the lens and the location of focus, r is the radius of aperture and σ is the spatial constant of point spread function.

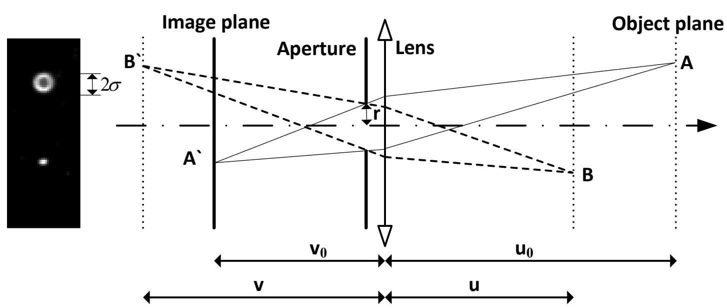

Figure 2 Geometry of defocused imaging

Fig. 2 shows the situation in which a lens system having a small f-number is used to project a point at a distance u onto an image plane at distance v_0. The point A appears focused on the image plane. The point B appears blurred on the image plane.

Given the configuration shown in Fig. 2, A.Pentland derived the formula [12]:

$$D_0 = \frac{Fv_0}{v_0 - F + \sigma kf} \tag{1}$$

where D_0 is the depth, f is the f-number of the camera lens, F is the focal length of the camera lens and k is a constant of proportionality. The basic limitation of this formula is that these parameters are based on the ideal thin lens model and in fact they can never be measured precisely on any camera. For this reason, equation (1) was modified as follow:

$$D == \frac{Fv_0}{v_0 - F + \sigma kf} q \tag{2}$$

where q is the compensation factor.

After particle depth measurement, the X-coordinate and Y-coordinate of particle position can be computed using equation (3) and equation (4), respectively.

$$x = u + \frac{D \times u \times s}{f} \tag{3}$$

$$y = v + \frac{D \times v \times s}{f} \tag{4}$$

where s is the pixel size of camera. In this case, s is set equal to 7.6 μm.

3. Basic Theories

Circular Hough Transform (CHT) is the method commonly used to detect circular objects and locate their centers. In [13], D.loannou applied the radius histogram to verify the existence of circular object and determine its radius. In this study, they are used to calculate the blur circle center and radius, respectively. In the real situation, the blur circle center and radius cannot be determined by CHT and radius histogram exactly due to distortion, noise and pixels missing from edge. For this issue, Quadrant Radius Histogram (QRH) was proposed, and it will be described in this section.

3.1. Circular Hough Transform

The Circular Hough Transform can be a very efficient approach for detecting circles and circular arcs, and locating the centers of circular objects [14-16]. CHT need just one parameter plane to store all the information for locating circles of various radiuses, which accumulates not just one point per edge pixel but whole line of points along the edge normal at each edge point location [16]. In fact, the line need not be extended indefinitely in either direction but only over the restricted range of radiuses on the blur circle. The peaks, which are corresponds to the blur circle centers, are located by direct searching in CHT parameter space.

3.2. Radius Histogram

In this section, we use the output of CHT as the blur circle center. The construction of radius histogram consists of five parts[13][16-18]: (1) choose one detected particle; (2) extract the square sub-region of particle edge image with the center placed at the blur circle center and the side length set equal to the maximum blur circle radius, as shown in Fig. 3; (3) calculate the distance between the sub-region center and the pixel over the sub-region; (4) compute the histogram of distance ("radius histogram"), as shown in Fig. 4; (5) the highest peak in the radius histogram, whose position corresponds to the blur circle radius, is detected.

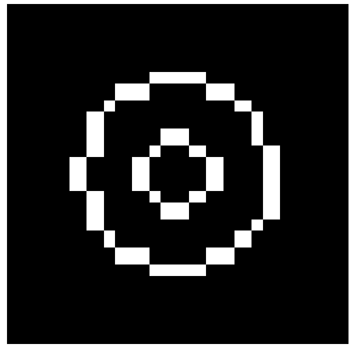

Figure 3 The extracted square sub-region of particle edge image

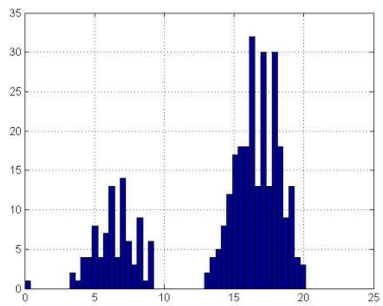

Figure 4 The radius histogram of blur circle

3.3. Quadrant Radius Histogram

Given the sub-region extracted in section 3.2, we compute the Quadrant Radius Histogram for it as follows [19][20]. We use the output of radius histogram in section 3.2 as the blur circle radius. Firstly, the sub-region is split into four quadrants, depicted in Fig. 5. Secondly, the radius histogram for each quadrant ("quadrant radius histogram") is computed, as shown in Fig. 6. Finally, the four highest peaks, whose positions correspond to four blur circle radiuses ("quadrant radius"), are detected in four quadrant radius histograms.

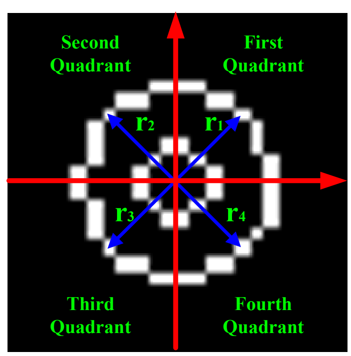

Figure 5 Four-quadrant split of extracted square sub-region

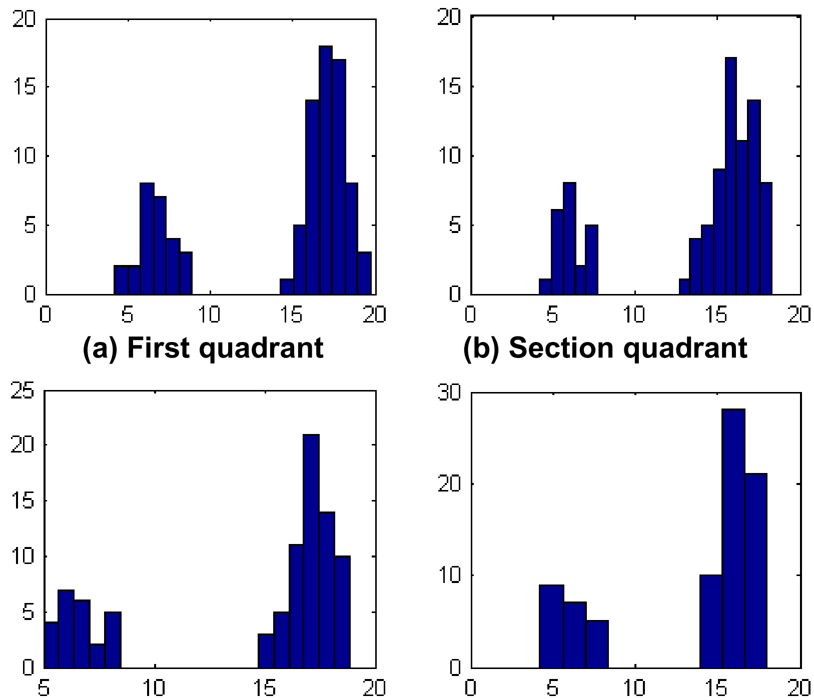

(a) First quadrant (b) Section quadrant

(c) Third quadrant (d) Fourth quadrant

Figure 6 Four quadrant radius histograms

4. Particle 3D position measurement

4.1. Particle center and radius update scheme

In the ideal case, the particle edge is the continuous circle. The center can be determined exactly by searching the highest peak in the CHT parameter space. In fact, because of digitization error, distortion of particle edge and pixels missing from the particle edge, the particle center cannot be determined accurately by direct searching. In this section, we use the result of analysis of QRH to update the particle center coordinate and radius, and then modify more accurately. The update scheme for the particle center coordinate and radius is stated as follows.

- Initialization
  - Initial particle center coordinate (u_i, v_i) ($i = 1,\ldots,N$, N is the number of detected particles) and radius r_i are obtained by using CHT and radius histogram
  - Four quadrant radiuses r_{1i}, r_{2i}, r_{3i} and r_{4i} are obtained by using QRH
- If $|r_{1i} - r_{2i}| \big/ (r_{1i} + r_{2i}) \geq 0.5$ then
  - $r_{1i} = \max(r_{1i}, r_{3i})$, $r_{3i} = \max(r_{1i}, r_{3i})$
- End {if}
- If $|r_{2i} - r_{4i}| \big/ (r_{2i} + r_{4i}) \geq 0.5$ then
  - $r_{2i} = \max(r_{2i}, r_{4i})$, $r_{4i} = \max(r_{2i}, r_{4i})$

- End {if}
- $r_i = mean(r_{1i} + r_{2i} + r_{3i} + r_{4i})$
- $u_i^' = u_i + r_{1i} - r_{3i}, v_i^' = v_i + r_{2i} - r_{4i}$
- $u_i = u_i^', v_i = v_i^'$

4.2. 3D particle position measurement procedure

In summary, the 3D particle position measurement is consisted of the following eight steps:

Step 1: Preprocess the particle image, and then detect the particle edge. In this approach, Sobel edge detection method is used to detect the particle edge, because it is able to estimate edge orientation to 1o and very simple to apply.

Step 2: Detect the blur circle and calculate the blur circle radius center coordinate (u_i^p, v_i^p) using CHT.

Step 3: Extract the square sub-region of the particle edge image with the center of region placed at the blur circle center (u_i^p, v_i^p) and the side length set equal to the maximum blur circle radius r_i, and then determine the blur circle radius r_p using radius histogram.

Step 4: Choose one of the detected particles, and set:

$$(u_i, v_i) = (u_i^p, v_i^p) \tag{5}$$

$$r_i = r_i^p \tag{6}$$

Step 5: Extract the square sub-region of the particle edge image with the center of region placed at the blur circle center (u_i, v_i) and the side length set equal to the blur circle radius r_i, and then construct the QRH.

Step 6: Analyze the QRH, and update the particle center coordinate (u_i, v_i) and radius r_i with the particle center and radius update scheme.

Step 7: Judge whether the iterative condition is met or not. If η is less than 10%, the algorithm is continued with next step. If not, (u_i, v_i) and radius r_i are set as the initial blur circle center and radius, respectively, and return to step 5.

$$\eta = \frac{|r_{1i} - r_{3i}| + |r_{2i} - r_{4i}|}{2} \times 100\% \tag{7}$$

where r_{1i}, r_{2i}, r_{3i} and r_{4i} are the four quadrant radiuses of the chosen particle.

Step 8: Calculate the particle depth using equation (2) with blur circle radius r_i, and then calculate the 2D particle position using equation (3) and (4).

Step 9: Label the chosen particle, and return to step 4 until all detected particles are labeled.

5. Implementation and results

5.1. Experimental setup and defocused particle image acquisition

We have employed an imaging system with a single CCD camera to capture different focused and defocused particle images. Fig. 6 illustrates the imaging system used in this study. In Fig. 6, L is the distance between the camera lens and its focal point, and R is the distance between the camera lens and the glass plate. They can be obtained by reading the scale on the optical rail. The tracer particles whose size is about 0.04 mm are placed on the glass plate at known coordinate positions. The glass plate is illuminated from the side with laser light. Particle images are captured with a CCD camera (IMPERX IPX-2M30-L). The focal length of the camera lens is set equal to 50 mm, and L is set equal to 450 mm. The captured image is digitized into 1600(H) $\times$ 1200(V) pixel with 8 bit gray level resolution.

After the camera calibration, particle images are captured at nine glass plate positions ranging from 450 mm to 410 mm at interval of -5 mm, as shown in Fig. 7. (In order to show clearly, we cut the image size 1600×1200 to 256×256). From Fig. 7, it is obvious that the particles are defocused on the image plane as the glass plate moves away from focal point.

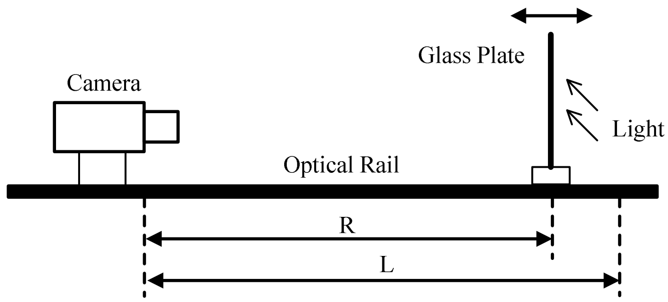

Figure 6 Experimental setup

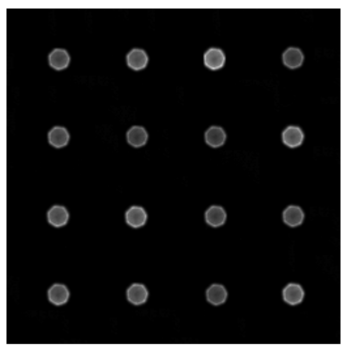

Figure 7 Experimental defocused particle image (R=410 mm)

5.2. Parameter estimation

The right-hand side of equation (2) contains two unknown parameters, k and q. If two different values of variable D and σ are known, we can solve the equations for k and q. In this study, the values of variable D and σ are measured by the defocus calibration procedure. Firstly, the two defocused particle images are captured with glass plate at two or more known positions. Secondly, the blur circle radius is calculated by using blur circle radius measurement algorithm mentioned above. Finally, the equations are solved for k and q.

5.3. The results and discussion

5.3.1. The particle radius measurement: The above computational method for computing the blur circle radius was implemented, and the mean and the standard deviation of blur circle radius were computed, respectively, as shown in Fig. 8 and Fig. 9.

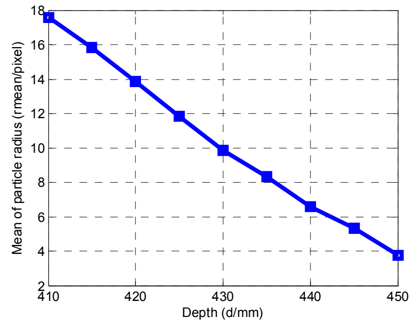

Figure 8 The mean of particle radius

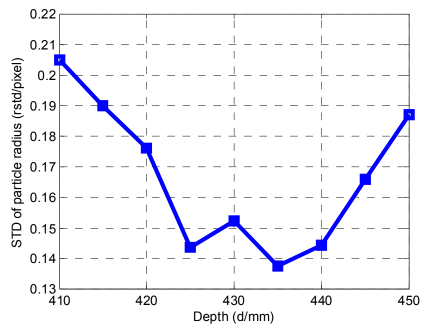

Figure 9 The standard deviation of particle radius

It can be seen that the particle radius increases approximately linearly with decreasing the depth in Fig. 8. From Fig. 9, if the depth is less than 430 mm the stand deviation of particle radius increases with increasing the depth, or, increases with decreasing the depth.

5.3.2. The particle 3D position measurement: We define e_x as the Mean Absolute Error (MAE) of x-coordinate, e_y as the MAE of y-coordinate and e_d as the MAE of depth. They are given as between:

$$e_x = \frac{1}{n}\sum_{i=1}^{n}\left|x_i - x_i^{'}\right| \quad (8)$$

$$e_y = \frac{1}{n}\sum_{i=1}^{n}\left|y_i - y_i^{'}\right| \quad (9)$$

$$e_d = \frac{1}{n}\sum_{i=1}^{n}\left|d_i - d_i^{'}\right| \quad (10)$$

where $x_i^{'}$, $y_i^{'}$ and $d_i^{'}$ are the X-coordinate, Y-coordinate and Z-coordinate of particle position which are known on the glass plate, n is the number of particles in the image plane. They are shown in Fig. 10 and Fig. 11.

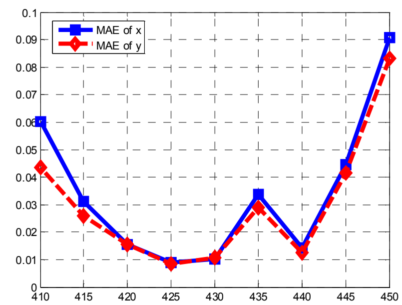

Figure 10 The MAE of X-coordinate and Y-coordinate

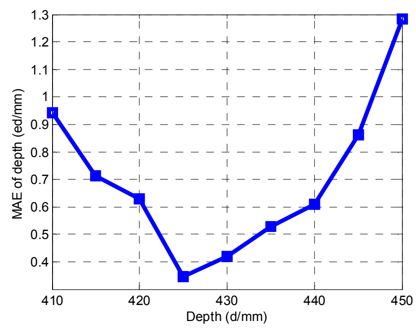

Figure 11 The MAE of depth

The MAE of X-coordinate and Y-coordinate are much less than the MAE of depth. The minimum MAE of depth is 0.18 mm, and the maximum MAE of depth is 1.27 mm.

Acknowledgement

This work was financially supported by National Natural Science Foundation of China (Grant No. 50879098).

References

[1] Kieft, R.N., Schreel, K.R.A.M., van der Plas, G.A.J., and Rindt, C.C.M.: 'The application of a 3D PTV algorithm to a mixed convection flow', Experiments in Fluids, 2002, 33, (4), pp. 603-611.

[2] Willneff, J.: '3D particle tracking velocimetry based on image and object space information'. ISPRS Commission V Symposium, International Archives of Photogrammetry, Remote Sensing and Information Sciences, Corfu, Greece, Sep 2002, pp. 1-6

[3] Hinsch, K.D.: 'Holographic particle image velocimetry'. 4th International Symposium on Particle Image Velocimetry, Gottingen, Germany, Sep 2001, pp. 61-72

[4] Willert, C.E., and Gharib, M.: 'Three-dimensional particle imagine with a single camera', Experiments in Fluids, 1992, 12, (6), pp. 353-358

[5] Pereira, F., and Gharib, M.: 'Defocusing digital particle image velocimetry and the three dimensional characterization of two-phase flows', Measurement Science and Technology, 2002, 13, (5), pp. 683-694

[6] Grohte, R.L., and Dabiri, D.: 'An improved three-dimensional characterization of defocusing digital particle image velocimetry based on a new imaging volume definition', Measurement Science and Technology, 2008, 19, (6), pp. 1-14

[7] Hain, R., and Kähler, C.J.: '3D3C time-resolved measurement with a single camera using optical aberrations'. 13th Int Symp on Application of Laser Techniques to Fluid Mechanics, Lisbon, Portugal, June 2006, pp. 1-9

[8] Cierpka, C., Segura, R., Hain, R., and Kähler, C.J.: 'A simple single camera 3C3D velocity measurement technique without errors due to depth of correlation and spatial averaging for micro-fluidics', Measurement Science and Technology, 2010, 21, (4), pp. 1-14

[9] Pham, D.T., and Aslantas, V.: 'Depth from defocusing using a neural network', Pattern Recognition, 1999, 32, (5), pp. 715-727

[10] Murata, S., and Kawamura, M.: 'Particle depth measurement based on depth-from-defocus', Optics and Laser Technology, 1999, 31, (1), pp. 95-102

[11] Lin, H.Y., and Gu, K.D.: 'Depth recovery using defocus blur at infinity'. 19th international conference on pattern recognition, Tampa, USA, Dec 2008, pp. 1068-1071

[12] Pentland, A.P.: 'A new sense for depth of field', IEEE Transactions on Pattern Analysis and Machine Intelligence, 1987, 9, (4), pp. 523-531

[13]Marcin, S., and Ignacy, D.: 'Circular object detection using a modified Hough Transform', International Journal of Applied Mathematics and Computer Science, 2008, 18, (1), pp. 85-91

[14] Weiliang, D., and James, Y.: 'A robust Hough Transform algorithm for determining the radiation centers of circular and rectangular fields', Physics in Medicine and Biology, 2009, 54, pp. 555-567

[15] Julien, C., Valérie, F., and Didier, V.: 'Optimization of an Hough Transform algorithm for the search of a center', Pattern Recognition, 2008, 41, (2), pp. 567-574

[16] Davies, E.R., 'Theory, Algorithms, Practicalities' (Elsevier Press, 2005, 3rd edn.), pp. 283-337

[17] Heung, S.K., and Jong, H.K.: 'A two step circle detection algorithm from the interesting chords', Pattern Recognition Letters, 2001, 22, (6-7), pp. 787-798

[18] Yuen, H.K., Princen, J., and Kittler, J.: 'Comparative study of Hough Transform methods for circle finding', Image and vision computing, 1990, 8, (1), pp. 71-77

[19] Danyu, L., Yu, C.,Wallapak, T., Johnny, W., Jung, H.O., and Piet, C.D.G.: 'Quadrant Coverage Histogram: A new method for measuring quality of colonoscopic procedures'. Proceedings of the 29th Annual International Conference of the IEEE EMBS Cité Internationale, Lyon, France, August 2007, pp. 23-26

[20] Moyer, A.C., Evans, J.L., and Powell, M.: 'Comparison of observed gale radius statistics', Meteorology and Atmospheric physics, 2007, 97, (1-4), pp. 41-55

Authors

Xiaoli Bao received the M.S. degree in communication and information system from Shenyang Ligong University, Shenyang, China, in 2009. He is currently working toward the Ph.D degree in Dalian University of Technology. His research interests include computer vision, image processing and pattern recognition.

Muguo Li received the B.S. degree in automatic engineering from Dalian University of Technology, Dalian, China, in 1978. He is currently a Professor with the State Key Laboratory of Coastal and Offshore Engineering, Dalian University of Technology. His research interests include computer vision, image processing, automatic control.